RSC Advances

PAPER

View Article Online
View Journal | View Issue

Cite this: *RSC Adv.*, 2022, **12**, 21111

Ancillary ligand effects on α-olefin polymerization catalyzed by zirconium metallocene: a computational study†

Yanan Zhao,[a] Xianming Xu,[c] Yulong Wang,[c] Tong Liu,[c] Hongpeng Li,[c] Yongjun Zhang,[c] Libo Wang,[c] Xiuhui Wang,[c] Simeng Zhao[c] and Yi Luo *[ab]

Received 20th May 2022
Accepted 18th July 2022

DOI: 10.1039/d2ra03180a

rsc.li/rsc-advances

The polymerization of α-olefins catalyzed by zirconium metallocene catalyst was systematically studied through experiments and density functional theory (DFT) calculations. Having achieved an agreement between theory and experiment, it was found that the effect of the catalyst ligand on the C=C insertion reaction was significantly greater than that on the β-H elimination reaction. Therefore, the molecular weight of polymers can be increased by improving the activity of the C=C insertion. In addition, in comparison with propylene, the chain length of α-olefins can directly affect the stereotacticity of polymerization products, owing to steric hindrance between the polymer chain and monomer.

Introduction

Poly-α-olefins (PAOs) are oligomers of linear α-olefins, which are used as base stocks for synthetic lubricants in automotive and industrial applications. Synthetic base stocks perform better than conventional mineral base stocks in terms of viscosity index, kinematic viscosity, pour point and volatility, thermal and oxidative stability, *etc.* Synthetic base stocks can be used to prepare all kinds of high-grade lubricating grease products.[1–3] PAO synthetic base oil plays a key role in cutting-edge technology fields such as the aerospace and military industries. It is also the key raw material in the production of high-grade lubricating oil used in advanced automobile, wind power, high-speed railway, intelligent manufacturing, and other industries.[4] At present, synthesis of PAO base oils is primarily carried out through the oligomerization of pure α-decenes by foreign companies.[5]

The appropriate selection of catalyst and reaction conditions can aid in the production of PAOs with tailor-made properties. Notably, a catalyst plays a key effect on the polymerization activity, molecular weight, and branching degree.[6] The commonly used catalysts for α-olefin polymerization mainly include Lewis acid catalysts, Ziegler Natta catalysts, metallocene catalysts, ionic liquid catalysts, *etc.*[7–16] Among them, Ziegler Natta catalysts are traditional and the most common catalyst for olefin polymerization.[17–19] However, because Ziegler Natta catalysts have multiple active sites, olefins have different growth rates at different sites of catalyst, and the various properties of polymerization cannot be effectively controlled.[20] In comparison to Ziegler–Natta, metallocene catalysts can control various important parameters, such as co-monomer distribution, molecular weight, molecular weight distribution, molecular architecture, stereo-specificity, degree of linearity, and branching of the polymer, due to the single active sites available on the metallocene catalysts.[20,21] Thus, metallocene catalysts (with group IV metal) have become a research hotspot in the recent years and have been applied in industrial production owing to their single reaction active center and high catalytic activity.[22,23] There are four types of metallocene catalysts commonly used: (a) monometallocene catalyst,[24–27] (b) constrained geometry catalysts (CGC),[28–30] (c) unbridged metallocene catalysts,[31,32] (d) bridged metallocene catalysts[33–35] (Fig. 1). Compared with other types of metallocene catalysts, rigid bridging groups of bridged metallocene catalysts can produce relatively stable spatial-specific stereoscopic effects on chain propagation and coordination monomers, affording synthesis polymers with high molecular weight and regular structure.[31,36] Moreover, the bridged rigid structure makes the connection between the metallocene ring and the transition metal more stable, and the metallocene ring does not slip at high temperatures.[37] Therefore, the bridged metallocene catalyst also shows high catalytic activity at high temperatures.[38,39] As has been reported in the literature,[40–43] different electronic or stereoscopic effects of catalyst ligands can significantly affect the polymerization performance, but the relationship between the ligand of group IV bridged metallocene catalysts and activity or the molecular weight of α-olefins (*e.g.* 1-decene), polymerization at the molecular level remains poorly understood.[44–50]

[a]*State Key Laboratory of Fine Chemicals, School of Chemical Engineering, Dalian University of Technology, Dalian, 116024, China. E-mail: luoyi010@petrochina.com.cn*

[b]*PetroChina Petrochemical Research Institute, Beijing, 102206, China*

[c]*Daqing Petrochemical Research Center of PetroChina, Daqing, 163714, China*

† Electronic supplementary information (ESI) available: Optimized cartesian coordinates of all stationary points together with their single-point energies (a.u.) in solution and the imaginary frequencies (cm^{-1}) of transition states (XYZ file). See https://doi.org/10.1039/d2ra03180a

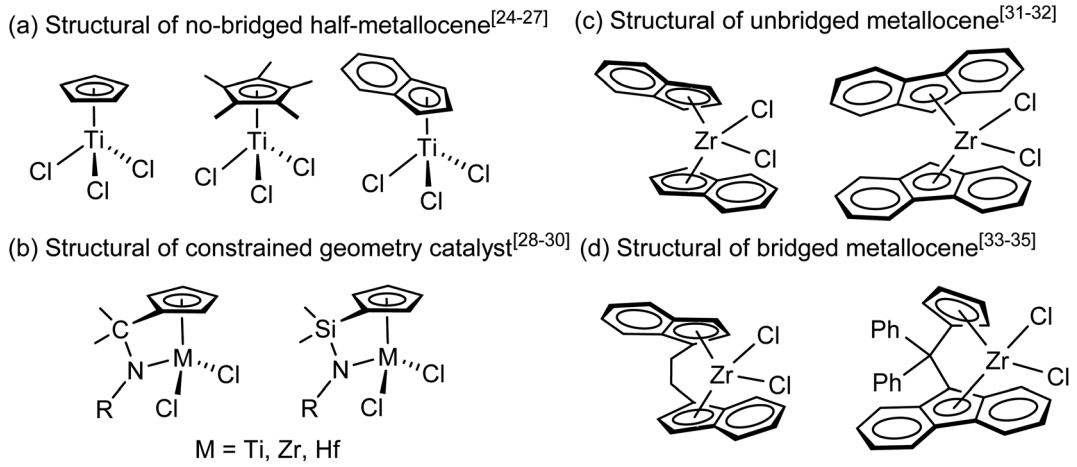

Fig. 1 Four common metallocene catalyst structures: (a) Monometallocene catalyst (b) Constrained Geometry Catalysts (CGC) (c) unbridged metallocene catalyst (d) bridged metallocene catalyst.

In general, the occurrence of polymerization requires MAO to activate the metallocene catalyst precursor (Fig. 1) to obtain active species with methyl groups, but the overall mechanisms of metallocene catalyst activation are not precisely understood. All computational studies dealing with the MAO activator suffer from its elusive structure, thus the use of DFT model systems is required (Fig. 2a). The starting point of this work was the activation of the dimethylated metallocene complexes, omitting the preceding catalyst alkylation step. This study mainly focuses on the systematic experimental comparison and theoretical calculation of the polymerization of 1-decene catalyzed by bridged metallocene complexes **1** (ref. 51) and **2** (ref. 52) (Fig. 2a) in order to explore the factors affecting both catalyst activity and polymer molecular weight. The research results will provide us with a theoretical basis for the design of high-efficiency catalysts. Four possible modes of olefin coordination insertion are shown in Fig. 2b. Therefore, the four different insertion modes were calculated and the results were compared, and the most favorable reaction path was selected for further analysis.

Computational details

All calculations were performed using the Gaussian 16 program.[53] The B3PW91 hybrid exchange-correlation functional was utilized for geometry optimization.[54–56] Each optimized structure was subsequently analyzed by harmonic vibration frequencies for the characterization of a minimum ($N_{imag} = 0$) or a transition state ($N_{imag} = 1$), providing thermodynamic data. The transition state structures were used to connect the reactant and product on either side *via* intrinsic reaction coordinate (IRC) tracking. The 6-31G* basis set was considered for C, H atoms. The Zr atoms were treated by the Stuttgart/Dresden effective core potential (ECP) and the associated basis sets.[57] This basis set was denoted as "BSI". Such a computational strategy has been widely used for the study of transition-metal containing systems.[58] To obtain more reliable relative energies, the single-point calculations of optimized structures were carried out at the level of M06 (ref. 59)/BSII, taking into account a solvation effect of toluene with the SMD[60] solvation model. In

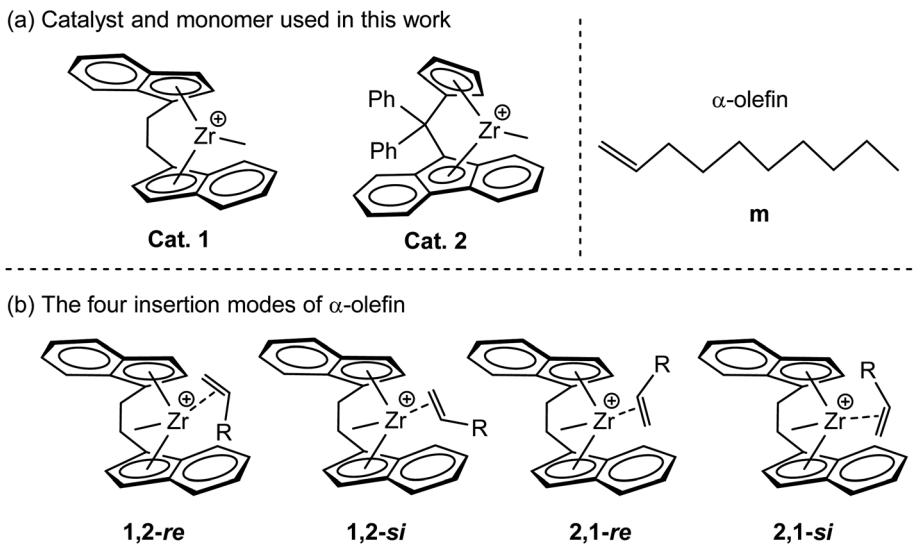

Fig. 2 (a) The structures of catalysts and monomers used for DFT calculation in this work (b) four possible modes of olefin coordination insertion.

the BSII, the 6-311G** basis set was used for the nonmetal atoms, whereas the basis sets together with associated pseudopotentials for Zr atoms were the same as that in geometry optimization. Therefore, unless otherwise mentioned, the free energy (ΔG, 298.15 K, 1 atm) in solution, which was used for the description of energy profiles, was obtained from solvation single-point calculation and gas-phase Gibbs free energy correction. The 3D molecular structures displayed herein were created using CYLview.[61]

Results and discussion

Catalyst **1** and catalyst **2** have been synthesized according to the procedure reported in the literature[51,52] and are applied for 1-decene (**m**) polymerization. The experimental results are summarized in Table 1. It can be seen from the experimental results that the activity and molecular weight of catalyst **2** for **m** are significantly higher than that of catalyst **1**. These differences in activity and molecular weight suggest that the ligand of the catalyst significantly influences the polymerization behavior of 1-decene. To systematically explore the factors affecting polymerization performance, density functional theory (DFT) calculations provided additional insight into the polymerization of **m** with catalysts **1** and **2**.

Effects of catalyst ligands on polymerization activity molecular weight

Firstly, four possible modes of **m** coordination insertion in **Cat.1** and **Cat.2** systems were calculated (Tables S1 and S2†). The computed results indicate that 1,2-insertion is both kinetically and thermodynamically more favorable than 2,1-insertion in the chain initiation stage. Based on this results, only 1,2-insertion mode was considered here for the chain propagation stage. Next, all kinetically favorable paths of chain initiation and chain growth stages are summarized in Fig. 3 and Fig. 4. As shown in Fig. 3, the average insertion barrier of **Cat.1** in the chain propagation (second to fourth monomer insertion) was 11.6 kcal mol^{-1}, which is 0.9 kcal mol^{-1} higher than that of **Cat.2** (10.7 kcal mol^{-1}, Fig. 4). These results are consistent with the experimental results shown above. In addition, For the rate-limiting step (first insertion), the energy barrier of **Cat.1** (12.1 kcal mol^{-1}) is slightly lower than that of **Cat.2** (12.9 kcal mol^{-1}), but the coordination complex of **Cat.1** (−0.7 kcal mol^{-1}) is significantly higher in energy than that of **Cat.2** (−3.2 kcal mol^{-1}). If taking **Cat.1** and **Cat. 2** as one system, one can roughly estimate the probability ratio of the occurring of the two rate-limiting steps *via* Boltzmann statistics[62] on the basis of the energies of the complexes and transition states. The result indicates that the insertion probability ratio of the first monomer by **Cat.1** and **Cat.2**, respectively, was calculated to be 5.4/94.6, suggesting the higher activity of **Cat.2** compared to **Cat.1**. Besides, the calculation results show that the isotactic polymers (*si-re-re-re*) can be obtained by **Cat.1** and **Cat.2** (Tables S1 and S2†). Moreover, the calculation results show that dispersion correction does not affect the energetic significantly in this work (Fig. 3 *vs.* S1†).

Table 1 Polymerization of 1-decene by catalyst **1** and **2**[a]

Cat. (μmol)	[Al] : [Zr]	Act.[b]	Mn[c]
1 (10)	50 : 1	6.3	6875
2 (10)	50 : 1	11.1	14 802

[a] Conditions: 1-decene, 200 mL; [B] : [Zr] = 1.5 : 1; 90 °C, 1 h. [b] 10^6 g (mol Cat.)$^{-1}$ M^{-1} h^{-1}. [c] kg mol^{-1}.

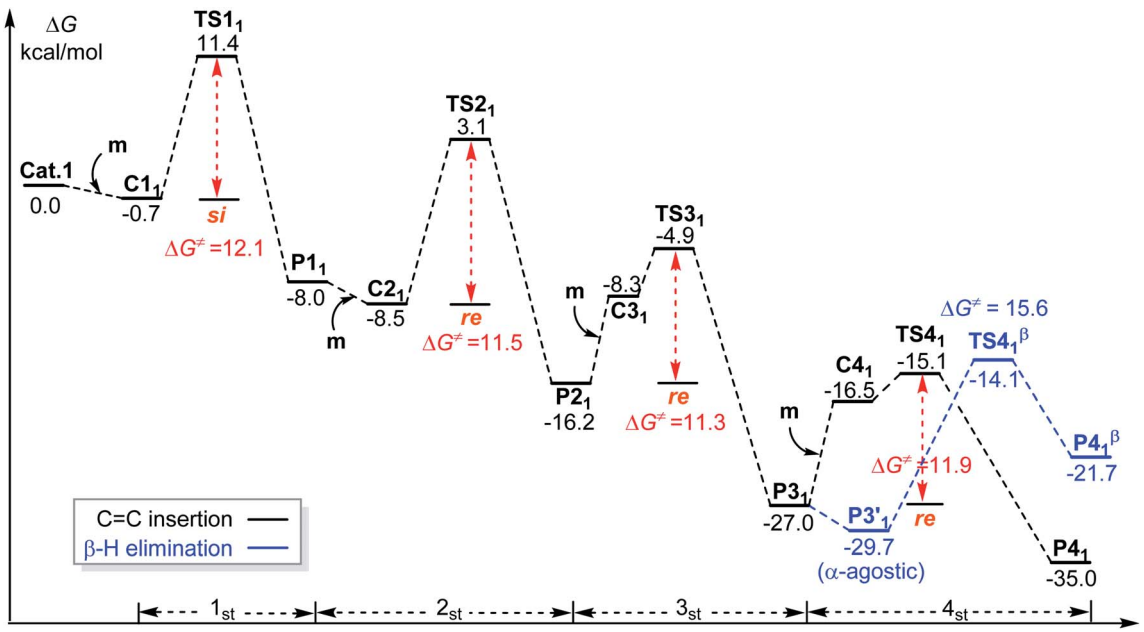

Fig. 3 Computed energy profiles for **Cat.1** mediated chain initiation and chain propagation of **m**. The C=C insertion and β-H elimination pathways are indicated in black and blue, respectively.

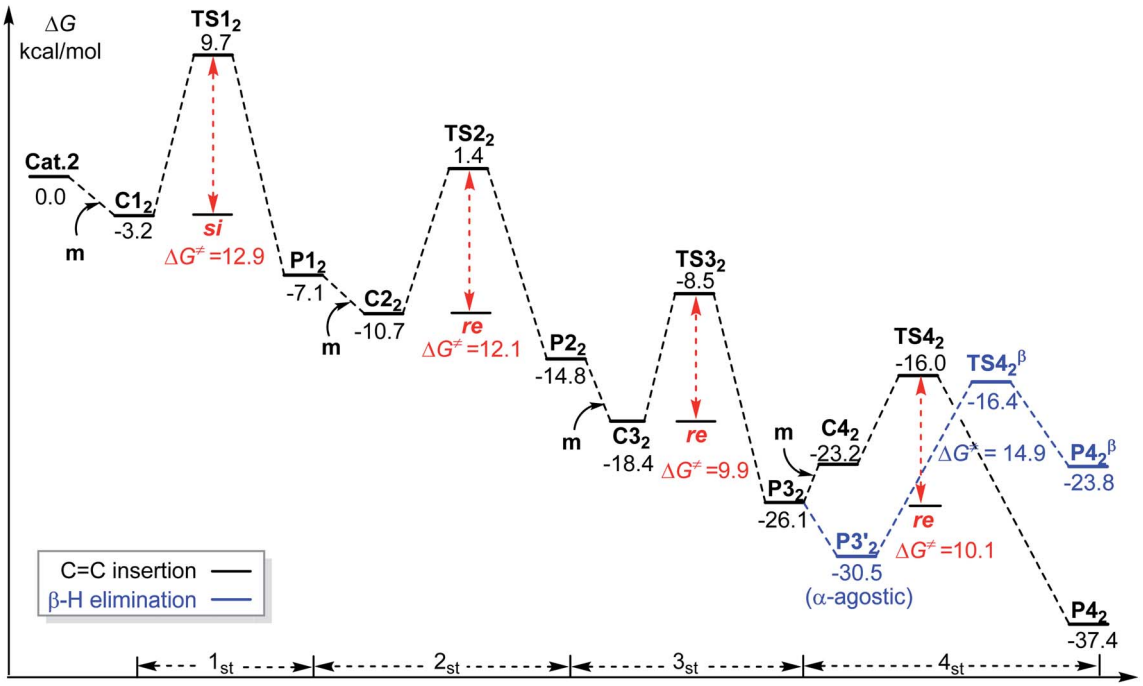

Fig. 4 Computed energy profiles for **Cat.2** mediated chain initiation and chain propagation of **m**. The C=C insertion and β-H elimination pathways are in black and blue, respectively.

Moreover, it can been seen that isomerization of the third molecule insertion product is always easier to occur than next **C=C** coordination (Fig. 3 and 4). It is worth noting that the formation of the **P3'$_1$** intermediate (−29.7 kcal mol^{-1}) is more favorable than the **m** coordination (**C4$_1$**, -16.5 kcal mol^{-1}) by more than 13 kcal mol^{-1} (Fig. 3), thus potential wells (**P3'$_1$**) may be formed to reduce the polymerization activity. However, for **Cat. 2**, it can be seen from Fig. 4 that the thermodynamic energy difference between **P3'$_2$** (−30.5 kcal mol^{-1}) and **C4$_2$** (−23.2 kcal mol^{-1}) is only 7.3 kcal mol^{-1}. At the same time, the β-H elimination is an obvious endothermic process, which makes the β-H elimination is less favorable than C=C insertion. Therefore, it can be further proved that the polymerization activity of **Cat. 2** is higher than that of **Cat. 1**, which can partially explain the experimental results.

To obtain a deeper insight into the activity difference in chain propagation, activation strain analysis[63] was performed for the corresponding two transition states (**TS4$_1$** and **TS4$_2$**, Fig. 5). For this purpose, the transition state (TS) structures were divided into two fragments, *viz.*, the catalyst part (cat.) and monomer moiety (mono). The energies of the fragments in the TS geometries were evaluated *via* single-point energy calculations. Such single-point energies of the fragments and the energy (corrected by BSSE) of the TS were used to estimate the interaction energy ΔE_{int} between the two fragments. The single-point energies, together with the energies of the respective fragments in their optimal geometries, allowed for the estimation of the distortion energies of the two fragments, ΔE_{strain}(cat.) and ΔE_{strain}(mono.). As the energy of TS, ΔE_{TS}, is evaluated with respect to the energy of the two separated fragments, the relation $\Delta E_{TS} = \Delta E_{int} + \Delta E_{strain}(cat.) + \Delta E_{strain}(mono.)$ holds. As shown in Fig. 5, in the case of **TS4$_1$**, the interaction energy ΔE_{int} was significantly stronger than that in **TS4$_2$** (−71.7 kcal mol^{-1} *vs.* −34.1 kcal mol^{-1}), but the total distortion energy of **TS4$_1$** was larger (67.2 kcal mol^{-1}). Therefore, **TS4$_1$** needed to overcome the higher energy barrier 11.9 kcal mol^{-1}. Therefore, the larger steric repulsion between the metal center and monomer moiety in **TS4$_1$** accounted for its lower stability in comparison with **TS4$_2$**.

When considering the polymerization behavior, it is necessary to clarify the nature of the monomer and active species. First, the frontier molecular orbital energy gap between **m** and two active species (**Cat.1** and **Cat.2**) was calculated. Generally, the reactivity is strongly influenced by the frontier molecular orbital energy gap of the two reactants: the smaller the energy gap between the two reactants, the higher the reaction activity. As shown in Fig. 6, the energy gap between **m** and **Cat.1** is significantly smaller than that between **m** and **Cat.2**; therefore, there is a relatively strong interaction between **m** and **Cat.1** in **TS4$_1$** (−71.7 kcal mol^{-1}). The difference in the reactivity between the two catalysts originates mainly from the steric hindrance effect. However, the difference in activity is not manifested in the topographical steric map analyses,[64] because buried volume %V_{Bur} of **Cat. 1** and **2** are close to each other (81.7 *vs.* 82.3, Fig. S2†). Therefore, in the subsequent sections, we will discuss the structures of the two transition states **TS4$_1$** and **TS4$_2$** in detail (Fig. 7). In **TS4$_1$**, the polymer chain has to be twisted to a certain extent for coordination and insertion of the next monomer, but the steric hindrance of the fused-ring on the ligand of **Cat.1** is large, resulting in a large repulsion between the polymer chain and the fused-ring. As such, **TS4$_1$** needs to overcome the higher energy barrier. However, one of the

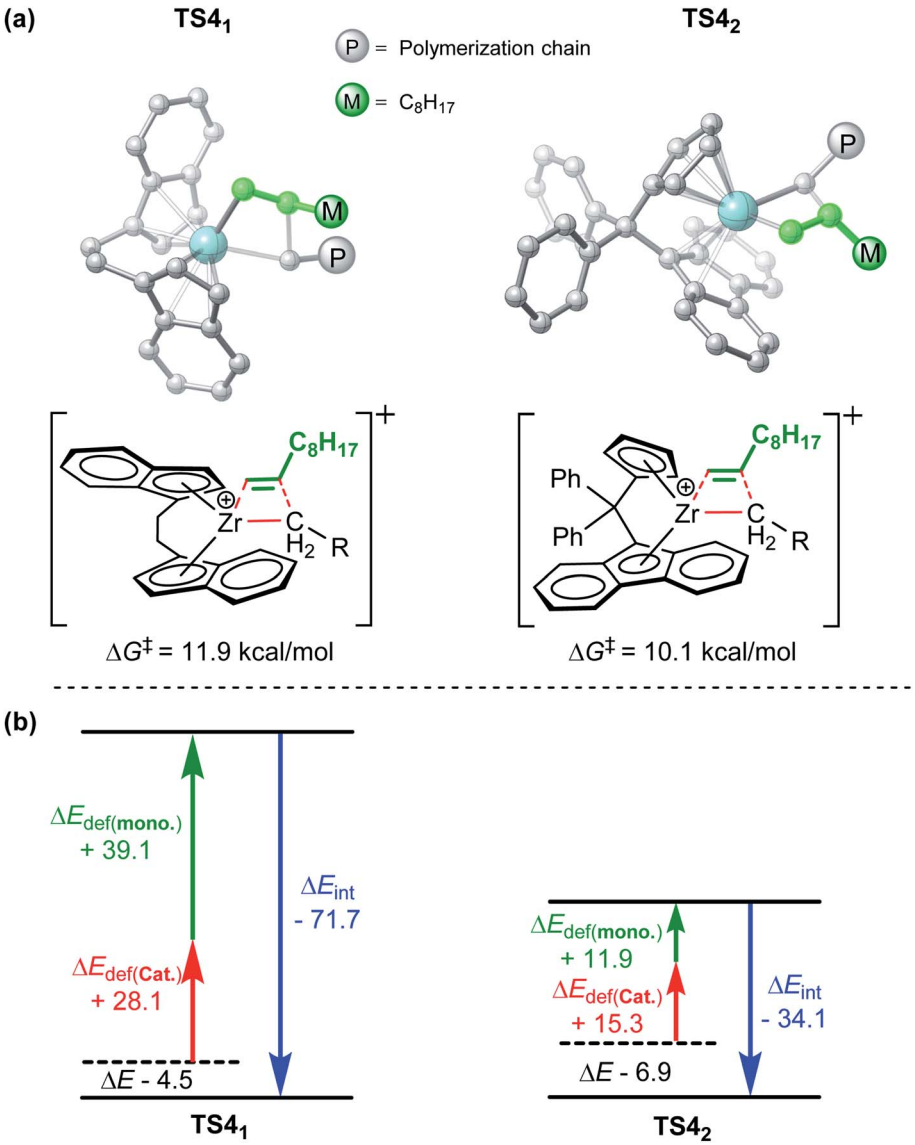

Fig. 5 Geometric structures (a) and activation strain analysis (b) of TS4$_1$ and TS4$_2$.

metallocene rings of **Cat.2** is cyclopentadienyl with small steric hindrance. The above-mentioned repulsion does not exist in this system, and thus, the energy barrier is relatively low. Consequently, the polymerization activity can be improved by reducing the repulsion between the ligands and polymer chains.

Next, the effects of different catalyst ligands on the molecular weight of polymers will be discussed. In general, the larger the energy barrier difference of the C=C insertion and β-H elimination, the higher the molecular weight of the polymerization products. In this study, the insertion of the fourth molecular monomer and β-H elimination based on the third insertion product mediated by **Cat.1** and **Cat.2** were investigated (Fig. 3 and 4). The results showed that when the catalyst was changed from **Cat.1** to **Cat.2**, the C=C insertion barrier decreased by 1.8 kcal mol^{-1} and the β-H elimination energy barrier decreased by 1.5 kcal mol^{-1}. As a result, the energy barrier difference

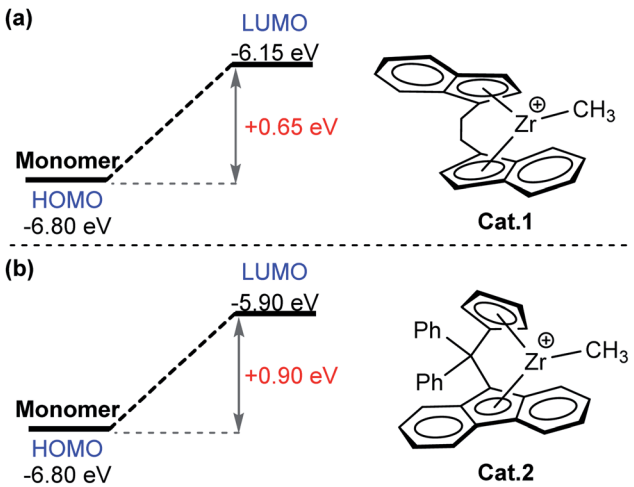

Fig. 6 Comparison of the frontier molecular orbital energy gap between m and **Cat.1**(a)/**Cat.2**(b).

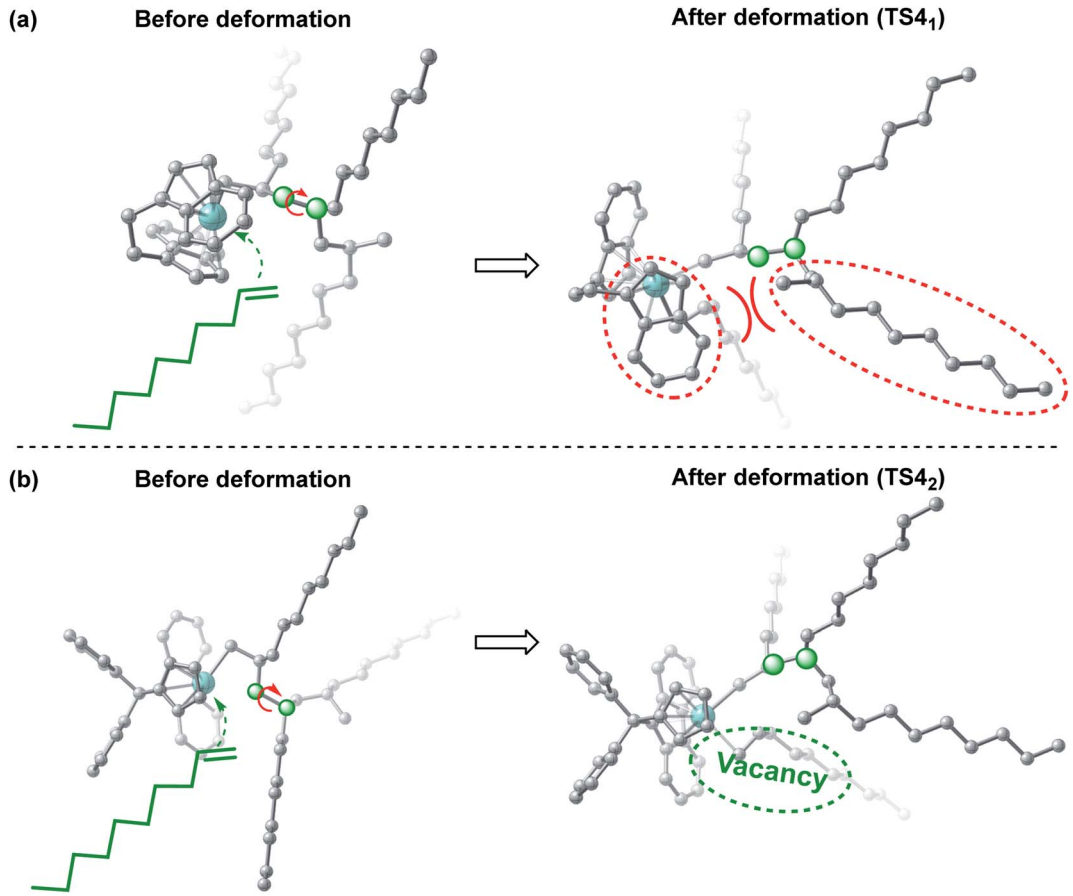

Fig. 7 Geometric deformation of the transition states TS4$_1$ and TS4$_2$.

between the C=C insertion and β-H elimination mediated by **Cat.2** was 0.3 kcal mol^{-1} higher than that by **Cat.1**, indicating that C=C insertion is relatively easier when using **Cat.2**. These results are consistent with the above-mentioned experimental results (Table 1). In addition, the effect of changing the ligand on C=C insertion is greater than that on β-H elimination. In other

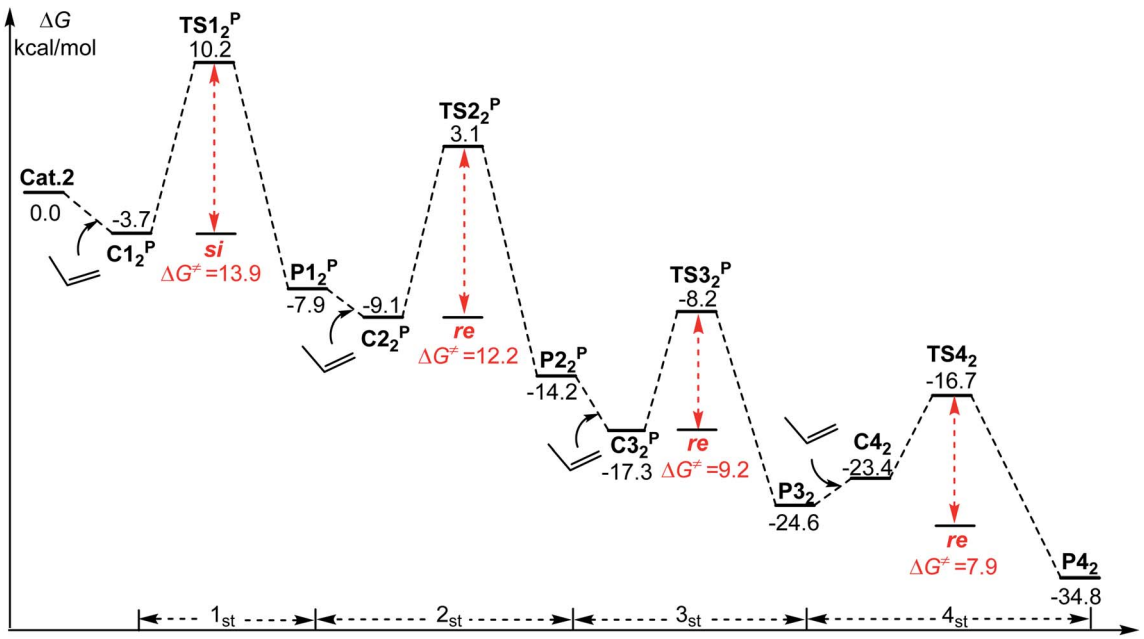

Fig. 8 Computed energy profiles for 2 mediated chain initiation and chain propagation of propylene.

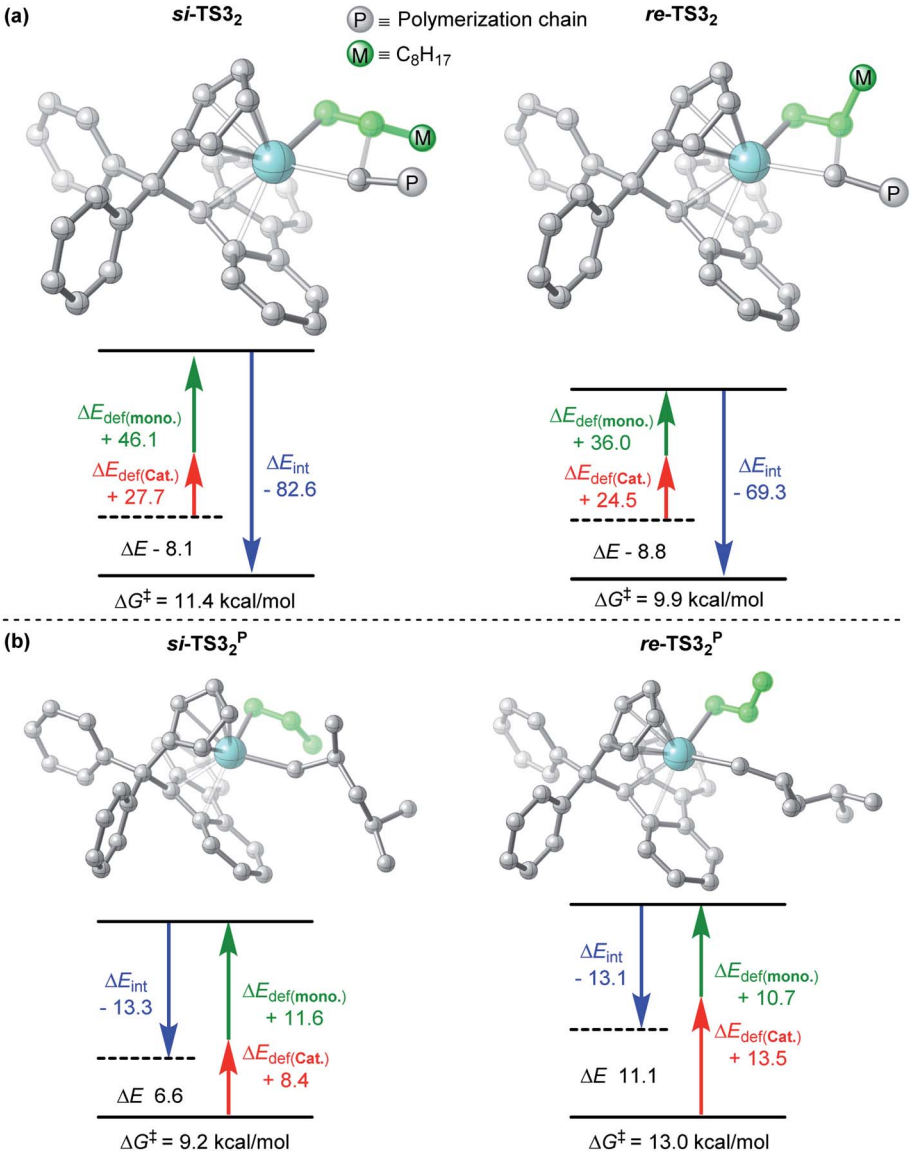

Fig. 9 Activation strain analysis of *si*-TS3$_2$, *re*-TS3$_2$, *si*-TS3$_2^P$ and *re*-TS3$_2^P$.

words, the molecular weight of the polymerization product can be increased by reducing the C=C insertion energy barrier.

Effect of monomer chain length on stereoselectivity

It has been reported in the literature[52] that a syndiotactic polymerization product can obtained through the polymerization of propylene catalyzed by **Cat.2**, which in contrast to what is mentioned above, that isotactic products can be obtained through the polymerization of **m** catalyzed using the same catalyst. To further understand the effect of the monomer chain length on stereoselectivity, propylene polymerization with **Cat.2** was conducted and the results are depicted in Fig. 8. The computational results are consistent with those reported in the literature,[52] and syndiotactic polymerization products (*si-re-si-re*) were obtained. Further, **m** and propylene showed different stereoselectivities at the third molecule insertion (*si-re-re-re vs. si-re-si-re*). Therefore, the activation strain analysis for the TSs of the third insertion (both **m** and propylene) was performed. As shown in Fig. 9a, in the case of ***re*-TS3$_2$**, the total distortion energy ΔE_{strain} is 60.5 kcal mol^{-1}, which could be partly balanced out by its ΔE_{int} (−69.3 kcal mol^{-1}) leading to a ΔE_{TS} of −8.8 kcal mol^{-1}. By contrast, a larger total distortion energy (ΔE_{strain} = 73.8 kcal mol^{-1}) in the ***si*-TS3$_2$** is difficult to be compensated by the interaction energy of −82.6 kcal mol^{-1}, thus producing a slightly higher ΔE_{TS} (***si*-TS3$_2$**, −8.1 kcal mol^{-1}). Therefore, the larger steric repulsion between the metal center and monomer moiety in ***si*-TS3$_2$** could account for its lower stability in comparison with ***re*-TS3$_2$**. In addition, as displayed in Fig. 9b, the interaction energy between the monomer and catalyst in ***si*-TS3$_2^P$** and ***re*-TS3$_2^P$** are almost the same, and the large total deformation energy of the monomer and catalyst in ***re*-TS3$_2^P$** is the primary reason for the higher energy barrier (13.0 kcal mol^{-1}).

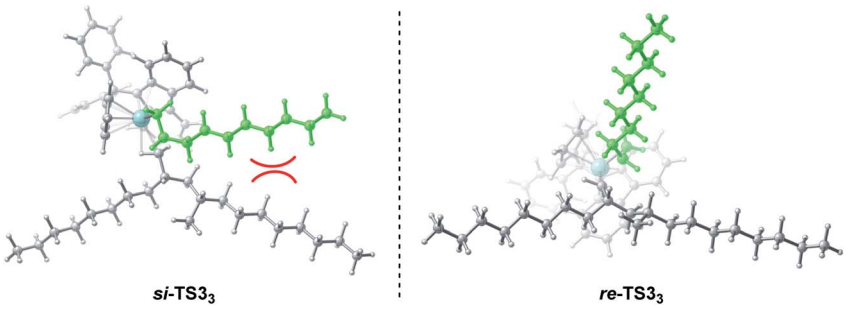

Fig. 10 Geometric structures of *si*-TS3$_3$ and *re*-TS3$_3$.

Based on the above-mentioned results, it was observed that the different types of stereoselectivity in the polymerization of **m** and propylene can be explained based on the steric hindrance between the catalyst and monomer. Therefore, by analyzing the geometric structure of the key transition states, the main causes of different deformations can be explored. As can be seen in Fig. 10, in ***si*-TS3$_3$**, due to the long monomer (**m**) and polymer chain, it is easy to produce a large repulsion between the monomer and polymer chain, resulting in a relatively high energy barrier (11.4 kcal mol^{-1}). However, in ***re*-TS3$_3$**, the relative orientation of monomer insertion is changed from *si* surface to *re* surface, effectively avoiding a large repulsion and lowering the energy barrier (9.9 kcal mol^{-1}). However, such a steric repulsion does not exist in propylene polymerization because the molecular chain of propylene is relatively short. Therefore, syndiotactic products can be obtained by the polymerization of propylene.

Conclusion

In summary, the origin of activity and molecular weight metallocene difference in the polymerization of 1-decene, catalyzed by various zirconium catalysts, have been computationally elucidated. The obtained results indicate that the effect of different catalyst ligands on β−H elimination is less than that on C=C insertion. Therefore, these systems can be used to indirectly regulate the molecular weight of polymerization products, by changing the energy barrier of the C=C insertion. The easier the C=C insertion, the higher the molecular weight of the polymerization product. Moreover, improving the activity of catalytic polymerization can be achieved by reducing the repulsion between the catalyst ligand and the polymer growth chain, such as reducing the steric hindrance of one aromatic ring of the catalyst. In addition, through the analysis of the transition state structure, the chain length of α-olefins will directly affect the stereoselectivity of polymerization products. When the length of the monomer is short, syndiotactic products are obtained, otherwise isotactic products are obtained. It is worth noting that, in practice, a polymerization reaction system is more complex. When the steric hindrance is regulated, the electronic factors may also change accordingly. Therefore, specific analysis must be carried out for specific systems.

Conflicts of interest

The authors declare no competing financial interest.

Acknowledgements

This work was partly supported by the NSFC (22101041, 22071015, U1862115) and China Postdoctoral Science Foundation (2021M700664). The authors also thank the RICC (RIKEN Integrated Cluster of Clusters) and the Network and Information Center of the Dalian University of Technology for part of the computational resources.

References

1 S. Ray, P. Rao and N. Choudary, Poly-α-Olefin-Based Synthetic Lubricants: A Short Review on Various Synthetic Routes, *Lubr. Sci.*, 2012, **24**, 23–44.
2 G. Yadav and N. Doshi, Development of a Green Process for Poly-α-Olefin Based Lubricants, *Green Chem.*, 2002, **4**, 528–540.
3 J. Hogg, A. Ferrer-Ugalde, F. Coleman and M. Swadźba-Kwaśny, Borenium Ionic Liquids as Alternative to BF_3 in Polyalphaolefins (PAOs) Synthesis, *ACS Sustainable Chem. Eng.*, 2019, **7**, 15044–15052.
4 M. Lahtela and T. Pakkanen, Molecular Modeling of Poly-α-olefin Synthetic Oils, *J. Phys. Chem.*, 1995, **99**, 10267–10271.
5 R. Leslie and L. Ronald *Synthetic Lubricants and High-Performance Functional Fluids[M]. Translated by Li P Q, Guan Z J, Geng Y J.*, China Petroleum Industrial Press, Beijing, 2006.
6 R. Shubkinand and M. Kerkemeyer, Tailor-making Polyalphaolefins, *Lubr. Sci.*, 2010, **8**, 115–134.
7 J. Baek, Y. Hyun, H. Lee, J. Lee, S. Bae, Y. Seo, D. Lee and B. Lee, Selective Trimerization of α-Olefins with Immobilized Chromium Catalyst for Lubricant Base Oils, *Catalysts*, 2020, **10**, 990–1012.
8 Q. Huang, L. Chen, L. Ma, Z. Fu and W. Yang, Synthesis and Characterization of Oligomer from 1-Decene Catalyzed by Supported Ziegler–Natta Catalyst, *Eur. Polym. J.*, 2005, **41**, 2909–2915.
9 Q. Huang, L. Chen, Y. Sheng, L. Ma, Z. Fu and W. Yang, Synthesis and Characterization of Oligomer from 1-Decene

Catalyzed by $AlCl_3/TiCl_4/SiO_2/Et_2AlCl$, *J. Appl. Polym. Sci.*, 2006, **101**, 584–590.

10 H. Shao, X. Gu, R. Wang, X. Wang, T. Jiang and X. Guo, Preparation of Lubricant Base Stocks with High Viscosity Index through 1-Decene Oligomerization Catalyzed by Alkylaluminum Chloride Promoted by Metal Chloride, *Energy Fuels*, 2020, **34**, 2214–2220.

11 C. Zhou, W. Li, M. Qiu, W. Li, H. Liu, H. Liu, K. Zhang and X. Chen, Precisely Regulating the Acidity of Mesoporous Silica on the Catalytic Performance of 1-Decene Oligomerization, *New J. Chem.*, 2021, **45**, 9109–9117.

12 R. Brüll, H. Pasch, H. Raubenheimer, R. Anderson and U. Wahner, Polymerization of Higher Linear α-Olefins with $(CH_3)_2Si$(2- methylbenz[e]indenyl)$_2ZrCl_2$, *J. Polym. Sci., Part A: Polym. Chem.*, 2000, **38**, 2333–2339.

13 I. Nifantev and P. Ivchenko, Fair Look at Coordination Oligomerization of Higher α-Olefins, *Polymers*, 2020, **12**, 1082–1113.

14 A. Jalali, M. Nekoomanesh, S. Dehghani and N. Bahri-Laleh, Effect of Metal Type on the Metallocene-Catalyzed Oligomerization of 1-Hexene and 1-Octene to Produce Poly α-Olefin-Based Synthetic Lubricants, *Appl. Organomet. Chem.*, 2019, e5338.

15 S. Dong, P. Mi, S. Xu, J. Zhang and R. Zhao, Preparation and Characterization of Single-Component Poly-α-olefin Oil Base Stocks, *Energy Fuels*, 2019, **33**, 9796–9804.

16 H. Shao, H. Li, J. Lin, T. Jiang, X. Guo and J. Li, Metallocene-Catalyzed Oligomerizations of 1-Butene and α-Olefins: Toward Synthetic Lubricants, *Eur. Polym. J.*, 2014, **59**, 208–217.

17 M. Masoori, M. Nekoomanesh, S. Posada-Pérez, R. Rashedi and N. Bahri-Laleh, Exploring Cocatalyst Type Effect on the Ziegler-Natta Catalyzed Ethylene Polymerizations: Experimental and DFT Studies, *J. Polym. Res.*, 2022, **29**, 197–208.

18 A. Piovano, M. D'Amore, K. Thushara and E. Groppo, Spectroscopic Evidences for $TiCl_4$/Donor Complexes on the Surface of $MgCl_2$-Supported Ziegler-Natta Catalysts, *J. Phys. Chem. C*, 2018, **122**, 5615–5626.

19 J. Kumawat and V. Gupta, Fundamental Aspects of Heterogeneous Ziegler-Natta Olefin Polymerization Catalysis: an Experimental and Computational Overview, *Polym. Chem.*, 2020, **11**, 6107–6128.

20 A. Shamiri, M. Chakrabarti, S. Jahan, M. Hussain, W. Kaminsky, P. Aravind and W. Yehye, The Influence of Ziegler-Natta and Metallocene Catalysts on Polyolefin Structure, Properties, and Processing Ability, *Materials*, 2014, **7**, 5069–5108.

21 S. Rahmatiyan, N. Bahri-Laleh, A. Hanifpour and M. Nekoomanesh-Haghighi, Different Behaviors of Metallocene and Ziegler-Natta Catalysts in Ethylene/1,5-Hexadiene Copolymerization, *Polym. Int.*, 2019, **68**, 94–101.

22 W. Kaminsky, Highly Active Metallocene Catalysts for Olefin Polymerization, *J. Chem. Soc., Dalton Trans.*, 1998, 1413–1418.

23 R. Stockland, S. Foley and R. Jordan, Reaction of Vinyl Chloride with Group 4 Metal Olefin Polymerization Catalysts, *J. Am. Chem. Soc.*, 2003, **125**, 796–809.

24 J. Huang, T. Wu and Y. Qian, Ethylene trimerization with a half-sandwich titanium complex bearing a pendant thienyl group, *Chem. Commun.*, 2003, 2816–2817.

25 K. Endo, T. Nomaguchi and Y. Tsuchiya, Control of Molecular Weight in Polymerization of Vinyl Chloride with $Cp^*Ti(OPh)_3$/MAO Catalyst, *J. Polym. Sci., Part A: Polym. Chem.*, 2010, **45**, 3872–3876.

26 K. Endo and M. Saitoh, Polymerization of Vinyl Chloride with $Cp^*Ti(OCH_3)_3$ -Methylaluminoxane Catalyst, *Polym. J.*, 2000, **32**, 300–302.

27 S. Gharajedaghi, Z. Mohamadnia, E. Ahmadi, M. Marefat, G. Pareras, S. Simon, A. Poater and N. Bahri-Laleh, Experimental and DFT Study on Titanium-based Half-Sandwich Metallocene Catalysts and their Application for Production of 1-Hexene from Ethylene, *Mol. Catal.*, 2021, **509**, 111636–111648.

28 J. McInnis, M. Delferro and T. Marks, Multinuclear Group 4 Catalysis: Olefin Polymerization Pathways Modified by Strong Metal–Metal Cooperative Effects, *Acc. Chem. Res.*, 2014, **47**, 2545–2557.

29 A. McKnight and R. Waymouth, Group 4 *ansa*-Cyclopentadienyl-Amido Catalysts for Olefin Polymerization, *Chem. Rev.*, 1998, **98**, 2587–2598.

30 U. Siemeling, Chelate Complexes of Cyclopentadienyl Ligands Bearing Pendant O-Donors, *Chem. Rev.*, 2000, **100**, 1495–1526.

31 H. Alt and A. Köpp, Effect of the Nature of Metallocene Complexes of Group IV Metals on Their Performance in Catalytic Ethylene and Propylene Polymerization, *Chem. Rev.*, 2000, **100**, 1205–1221.

32 A. Zhou, Y. Zhang, Y. Shia and Q. Xu, Integrated Synthesis of Metallocene@support Catalysts Based on Glyphosate and its Zirconium Derivatives, *RSC Adv.*, 2017, **7**, 55866–55873.

33 W. Kaminsky, K. Kiilper, H. Brintzinger and F. Wild, Polymerization of Propene and Butene with a Chid Zirconocene and Methylalumoxane as Cocatalyst, *Angew. Chem., Int. Ed.*, 1985, **24**, 507–508.

34 J. Eisch, F. Owuor and P. Otieno, Metalations with Group 4 Alkylmetal(IV) Halides: Expeditious Route to Metallocene and Nonmetallocene Procatalysts, *Organometallics*, 2001, **20**, 4132–4134.

35 J. Buffet, T. Arnold, Z. Turner, P. Angpanitcharoen and D. O'Hare, Synthesis and Characterisation of Permethylindenyl Zirconium Complexes and Their Use in Ethylene Polymerization, *RSC Adv.*, 2015, **5**, 87456–87464.

36 F. Wild, L. Zsolnai, G. Huttner and H. Brintzinger, Synthesis and Molecular Structures of Chiral *ansa*-Titanocene Derivatives with Bridged Tetrahydroindenyl Ligands, *J. Organomet. Chem.*, 1982, **232**, 233–247.

37 F. Wild, M. Wasiucionek, G. Huttner and H. Brintzinger, Synthesis and Crystal Structure of a Chiral ansa-Zirconocene Derivative with Ethylene-Bridged Tetrahydroindenyl Ligands, *J. Organomet. Chem.*, 1985, **288**, 63–67.

38 C. Zuccaccia, N. Stahl, A. Macchioni, M. Chen, J. Roberts and T. Marks, NOE and PGSE NMR Spectroscopic Studies of Solution Structure and Aggregation in Metallocenium Ion-Pairs, *J. Am. Chem. Soc.*, 2004, **126**, 1448–1464.

39 F. Song, S. Lancaster, R. Cannon, M. Schormann, S. Humphrey, C. Zuccaccia, A. Macchioni and M. Bochmann, Synthesis, Ion Aggregation, Alkyl Bonding Modes, and Dynamics of 14-Electron Metallocenium Ion Pairs $[(SBI)MCH_2SiMe^{3+}\cdots, X^-]$ (M = Zr, Hf): Inner-Sphere (X = $MeB(C_6F_5)_3$) versus Outer-Sphere (X = $B(C_6F_5)_4$) Structures and the Implications for "Continuous" or "Intermittent" Alkene Polymerization Mechanisms, *Organometallics*, 2005, **24**, 1315–1328.

40 Y. Zhao, H. Lu, G. Luo, X. Kang, Z. Hou and Y. Luo, Origin of Stereoselectivity and Multidimensional Quantitative Analysis of Ligand Effects on Yttrium Catalysed Polymerization of 2-Vinylpyridine, *Catal. Sci. Technol.*, 2019, **9**, 6227–6233.

41 C. Wang, G. Luo, M. Nishiura, G. Song, A. Yamamoto, Y. Luo and Z. Hou, Heteroatom-Assisted Olefin Polymerization by Rare-Earth Metal Catalysts, *Sci. Adv.*, 2017, **3**, e1701011.

42 X. Wang, F. Lin, J. Qu, Z. Hou and Y. Luo, DFT Studies on Styrene Polymerization Catalyzed by Cationic Rare-Earth-Metal Complexes: Origin of Ligand-Dependent Activities, *Organometallics*, 2016, **35**, 3205–3214.

43 A. Kronast, D. Reiter, P. Altenbuchner, S. Vagin and B. Rieger, 2-Methoxyethylamino-bis(phenolate) yttrium Catalysts for the Synthesis of Highly Isotactic Poly(2-vinylpyridine) by Rare-Earth Metal-Mediated Group Transfer Polymerization, *Macromolecules*, 2016, **49**, 6260–6267.

44 A. Laine, B. Coussens, J. Hirvi, A. Berthoud, N. Friederichs, J. Severn and M. Linnolahti, Effect of Ligand Structure on Olefin Polymerization by a Metallocene/Borate Catalyst: A Computational Study, *Organometallics*, 2015, **34**, 2415–2421.

45 S. Karimia, N. Bahri-Laleha, G. Parerasb, S. Sadjadic, M. Nekoomanesh-Haghighia and A. Poater, Pd on Nitrogen Rich Polymer-Halloysite Nanocomposite as an Environmentally Benign and Sustainable Catalyst for Hydrogenation of Polyalfaolefin based Lubricants, *J. Ind. Eng. Chem.*, 2021, **97**, 441–451.

46 M. D'Alterio, C. Rosa and G. Talarico, Stereoselective Lactide Polymerization: the Challenge of Chiral Catalyst Recognition, *ACS Catal.*, 2020, **10**, 2221–2225.

47 A. Hanifpour, N. Bahri-Laleh, M. Nekoomanesh-Haghighi and A. Poater, Coordinative Chain Transfer Polymerization of 1-Decene in the Presence of A Ti-Based Diamine Bis(phenolate) Catalyst: A Sustainable Approach to Produce Low Viscosity PAOs, *Green Chem.*, 2020, **22**, 4617–4626.

48 M. Tabrizi, S. Sadjadi, G. Pareras, M. Nekoomanesh-Haghighi, N. Bahri-Laleh and A. Poater, Efficient Hydro-Finishing of Polyalfaolefin Based Lubricants under Mild Reaction Condition using Pd on Ligands Decorated Halloysite, *J. Colloid Interface Sci.*, 2021, **581**, 939–953.

49 A. Hanifpoura, N. Bahri-Laleha, M. Nekoomanesh-Haghighia and A. Poater, Group IV Diamine Bis(Phenolate) Catalysts for 1-Decene Oligomerization, *Mol. Catal.*, 2020, **493**, 111047.

50 A. Hanifpour, N. Bahri-Laleh, M. Nekoomanesh-Haghighi and A. Poater, 1-Decene Oligomerization by New Complexes Bearing Diamine-Diphenolates Ligands: Effect of Ligand Structure, *Appl. Organomet. Chem.*, 2021, **35**, e6227.

51 I. Lee, W. Gauthier, J. Ball, B. Iyengar and S. Collins, Electronic Effects in Ziegler-Natta Polymerization of Propylene and Ethylene Using Soluble Metallocene Catalysts, *Organometallics*, 1992, **11**, 2115–2122.

52 A. Razavi and J. Atwood, Preparation and Crystal Structures of the Complexes $(\eta^5\text{-}C_5H_4CPh^2\text{-}\eta^5\text{-}C_{13}H_8)MCl_2$, (M = Zr, Hf) and the Catalytic Formation of High Molecular Weight High Tacticity Syndiotactic Polypropylene, *J. Organomet. Chem.*, 1993, **459**, 117–123.

53 M. J. Frisch, G. W. Trucks, H. B. Schlegel, G. E. Scuseria, M. A. Robb, J. R. Cheeseman, G. Scalmani, V. Barone, G. A. Petersson, H. Nakatsuji, X. Li, M. Caricato, A. V. Marenich, J. Bloino, B. G. Janesko, R. Gomperts, B. Mennucci, H. P. Hratchian, J. V. Ortiz, A. F. Izmaylov, J. L. Sonnenberg, D. Williams-Young, F. Ding, F. Lipparini, F. Egidi, J. Goings, B. Peng, A. Petrone, T. Henderson, D. Ranasinghe, V. G. Zakrzewski, J. Gao, N. Rega, G. Zheng, W. Liang, M. Hada, M. Ehara, K. Toyota, R. Fukuda, J. Hasegawa, M. Ishida, T. Nakajima, Y. Honda, O. Kitao, H. Nakai, T. Vreven, K. Throssell, J. A. Montgomery Jr., J. E. Peralta, F. Ogliaro, M. J. Bearpark, J. J. Heyd, E. N. Brothers, K. N. Kudin, V. N. Staroverov, T. A. Keith, R. Kobayashi, J. Normand, K. Raghavachari, A. P. Rendell, J. C. Burant, S. S. Iyengar, J. Tomasi, M. Cossi, J. M. Millam, M. Klene, C. Adamo, R. Cammi, J. W. Ochterski, R. L. Martin, K. Morokuma, O. Farkas, J. B. Foresman and D. J. Fox, *Gaussian 16, Revision A.03*, Gaussian, Inc., Wallingford, CT, 2016.

54 A. Becke, Density-Functional Thermochemistry. III. The Role of Exact Exchange, *J. Chem. Phys.*, 1993, **98**, 5648–5653.

55 C. Lee, W. Yang and R. Parr, Development of the Colic-Salvetti Correlation-Energy Formula into A Functional of the Electron Density, *Phys. Rev. B*, 1988, **37**, 785–789.

56 J. Perdew, K. Burke and Y. Wang, Generalized Gradient Approximation for the Exchange-Correlation Hole of a Many-Electron System, *Phys. Rev. B*, 1996, **54**, 16533–16539.

57 (*a*) P. Hay and W. Wadt, *Ab Initio* Effective Core Potentials for Molecular Calculations. Potentials for the Transition Metal Atoms Sc to Hg, *J. Chem. Phys.*, 1985, **82**, 270–283; (*b*) P. Hay and W. Wadt, *Ab Initio* Effective Core Potentials for Molecular Calculations. Potentials for K To Au Including the Outermost Core Orbitals, *J. Chem. Phys.*, 1985, **82**, 299–310; (*c*) W. Wadt and P. Hay, *Ab Initio* Effective Core Potentials for Molecular Calculations. Potentials for Main Group Elements Na to Bi, *J. Chem. Phys.*, 1985, **82**, 284–298.

58 (*a*) Y. Zhao, G. Luo, X. Wang, X. Kang, D. Cui, Z. Hou and Y. Luo, DFT Studies on the Polymerization of Functionalized Styrenes Catalyzed by Rare-Earth-Metal Complexes: Factors Affecting C-H Activation Relevant to Step-Growth Polymerization, *Organometallics*, 2018, **37**, 3210–3218; (*b*) Y. Zhao, G. Luo, X. Kang, F. Guo, X. Zhu,

R. Zheng, Z. Hou and Y. Luo, "C–H…π Interaction" Regulates the Stereoselectivity in Olefin Polymerization, *Chem. Commun.*, 2019, **55**, 6689–6692; (*c*) L. Perrin, F. Bonnet, M. Visseaux and L. Maron, A DFT Study of Conjugated Dienes Polymerization Catalyzed by $[Cp^*ScR]^+$: Insights into the Propensity for *cis*-1,4 Insertion, *Chem. Commun.*, 2010, **46**, 2965–2967; (*d*) L. Perrin, F. Bonnet, T. Chenal, M. Visseaux and L. Maron, A Joint Experimental/Theoretical Investigation of the Statistical Olefin/Conjugated Diene Copolymerization Catalyzed by a Hemi-Lanthanidocene $[(Cp^*)(BH_4)LnR]$, *Chem.–Eur. J.*, 2010, **16**, 11376–11385.

59 (*a*) Y. Zhao and D. Truhlar, Benchmark Energetic Data in a Model System for Grubbs II Metathesis Catalysis and their Use for the Development, Assessment, and Validation of Electronic Structure Methods, *J. Chem. Theory Comput.*, 2009, **5**, 324–333; (*b*) Y. Zhao and D. Truhlar, The M06 Suite of Density Functionals for Main Group Thermochemistry, Thermochemical Kinetics, Noncovalent Interactions, Excited States, and Transition Elements: Two New Functionals and Systematic Testing of Four M06-Class Functionals and 12 Other Functionals, *Theor. Chem. Acc.*, 2008, **120**, 215–241.

60 A. Marenich, C. Cramer and D. Truhlar, Performance of SM6, SM8, and SMD on the SAMPL1 Test Set for the Prediction of Small-Molecule Solvation Free Energies, *J. Phys. Chem. B*, 2009, **113**, 4538–4543.

61 C. Y. Legault, *CYLview, 1.0b*, Université de Sherbrooke, 2009, **http://www.cylview.org**.

62 Y. Luo, Y. Luo, J. Qu and Z. Hou, QM/MM Studies on Scandium-Catalyzed Syndiospecific Copolymerization of Styrene and Ethylene, *Organometallics*, 2011, **30**, 2908–2919.

63 (*a*) F. Bickelhaupt and K. Houk, Analyzing Reaction Rates with the Distortion/Interaction-Activation Strain Model, *Angew. Chem., Int. Ed.*, 2017, **56**, 10070–10086; (*b*) I. Fernández and F. Bickelhaupt, Bioorthogonal Cycloadditions: Computational Analysis with the Distortion/Interaction Model and Predictions of Reactivities, *Chem. Soc. Rev.*, 2014, **43**, 4953–4967; (*c*) F. Liu, Y. Liang and K. Houk, Bioorthogonal Cycloadditions: Computational Analysis with the Distortion/Interaction Model and Predictions of Reactivities, *Acc. Chem. Res.*, 2017, **50**, 2297–2308; (*d*) K. Kitaura and K. Morokuma, A New Energy Decomposition Scheme for Molecular Interactions within the Hartree-Fock Approximation, *Int. J. Quantum Chem.*, 1976, **10**, 325–340.

64 (*a*) L. Falivene, R. Credendino, A. Poater, A. Petta, L. Serra, R. Oliva, V. Scarano and L. Cavallo, SambVca 2. A Web Tool for Analyzing Catalytic Pockets with Topographic Steric Maps, *Organometallics*, 2016, **35**, 2286–2293; (*b*) L. Falivene, Z. Cao, A. Petta, L. Serra, A. Poater, R. Oliva, V. Scarano and L. Cavallo, Towards the Online Computer-Aided Design of Catalytic Pockets, *Nat. Chem.*, 2019, **11**, 872–880, see **https://www.molnac.unisa.it/OMtools/sambvca2.1/index.html**.